Inorganic Chemistry

Article

pubs.acs.org/IC

Encapsulation of Two Potassium Cations in Preyssler-Type Phosphotungstates: Preparation, Structural Characterization, Thermal Stability, Activity as an Acid Catalyst, and HAADF-STEM Images

Akio Hayashi,[†] Hiromi Ota,[‡] Xavier López,[§] Norihito Hiyoshi,[∥] Nao Tsunoji,[†] Tsuneji Sano,[†] and Masahiro Sadakane*[,†]

[†]Department of Applied Chemistry, Graduate School of Engineering, Hiroshima University, 1-4-1 Kagamiyama, Higashi-Hiroshima 739-8527, Japan

[‡]Division of Instrumental Analysis, Department of Instrumental Analysis and Cryogenics, Advanced Science Research Center, Okayama University, 3-1-1 Tsushima-Naka, Kita-ku, Okayama 700-8530, Japan

[§]Departament de Química Física i Inorgànica, Universitat Rovira i Virgili, c/Marcel·lí Domingo 1, 43007 Tarragona, Spain

[∥]Research Institute for Chemical Process Technology, National Institute of Advanced Industrial Science and Technology (AIST), 4-2-1 Nigatake, Miyagino, Sendai 983-8551, Japan

Supporting Information

ABSTRACT: Dipotassium cation (K^+)-encapsulated Preyssler-type phosphotungstate, $[P_5W_{30}O_{110}K_2]^{13-}$, was prepared by heating monobismuth (Bi^{3+})-encapsulated Preyssler-type phosphotungstate, $[P_5W_{30}O_{110}Bi(H_2O)]^{12-}$, in acetate buffer in the presence of an excess amount of potassium cations. Characterization of the isolated potassium salt, $K_{13}[P_5W_{30}O_{110}K_2]$ (**1a**), and its acid form, $H_{13}[P_5W_{30}O_{110}K_2]$ (**1b**), by single crystal X-ray structure analysis, ^{31}P and ^{183}W nuclear magnetic resonance (NMR), Fourier transform infrared (FT-IR) spectroscopy, cyclic voltammetry (CV), high-resolution electrospray ionization mass spectroscopy (HR-ESI-MS), and elemental analysis revealed that two potassium cations are encapsulated in the Preyssler-type phosphotungstate molecule with formal D_{5h} symmetry, which is the first example of a Preyssler-type compound with two encapsulated cations. Incorporation of two potassium cations enhances the thermal stability of the potassium salt, and the acid form shows catalytic activity for hydration of ethyl acetate. Packing of the Preyssler-type molecules was observed by high-resolution high-angle annular dark-field scanning transmission electron microscopy (HAADF-STEM).

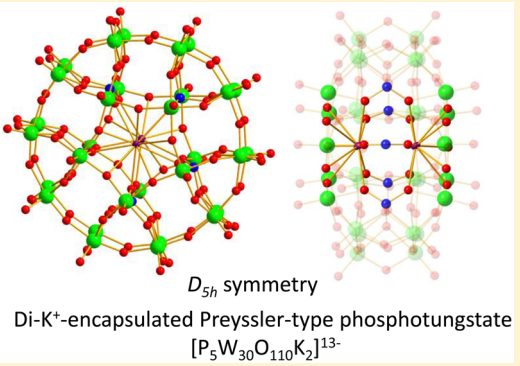

INTRODUCTION

Heteropolytungstates are anionic mixed metal-oxide clusters with tungsten as the main metal. They have been attracting increasing interest because of their multielectronic redox activities, acidic properties, and photochemical properties, and they have been utilized as catalysts and functional materials.[1−3] Among the various heteropolytungstates, Preyssler-type phosphotungstates, $[P_5W_{30}O_{110}M^{n+}(H_2O)]^{(15-n)-}$ (M: Na^+, Ca^{2+}, Bi^{3+}, Y^{3+}, lanthanoid cations, etc.), where five PO_4 tetrahedra are surrounded by 30 WO_6 octahedra to form a doughnut-shaped molecule, have been applied as acid catalysts and components in organic-polyoxometalate hybrid materials (Figure 1(a) and (b)). One of the most interesting features is that Preyssler compounds can encapsulate various cations, such as Na^+,[4,5] Ag^+,[6] K^+,[7,8] most lanthanoid cations,[5,9−13] Ca^{2+},[5,13,14] Bi^{3+},[5,13,15] Y^{3+},[5,13,14] and actinoid metals,[5,9,10,14,16] and their properties, such as redox potentials, magnetic properties, and thermal stability, are tunable by replacing encapsulated cations.[5,10,11,13,17−23] In all cases, only one cation is encapsulated in one Preyssler molecule, and the cation is coordinated by five oxygens (O_a) bound to P, five bridging oxygens (O_b) between two cap tungstens, and one water molecule (Figure 1(c) and (d)), and the symmetry of the molecules is therefore decreased from D_{5h} without encapsulated cations to C_{5v} by introducing one encapsulated cation. In the case of Preyssler-type sulfotungstate, one K^+ is located in the center of the molecules where K^+ is coordinated by 10 oxygens (O_a) bound to 5 P and no water molecule is coordinating to the encapsulated K^+.[24]

In the course of our research on Preyssler-type phosphotungstates,[13,15,25] we found a new compound with two encapsulated K^+. This is the first example of a Preyssler-type compound with two encapsulated metal cations. Thermal

Received: September 7, 2016

DOI: 10.1021/acs.inorgchem.6b02116
Inorg. Chem. XXXX, XXX, XXX−XXX

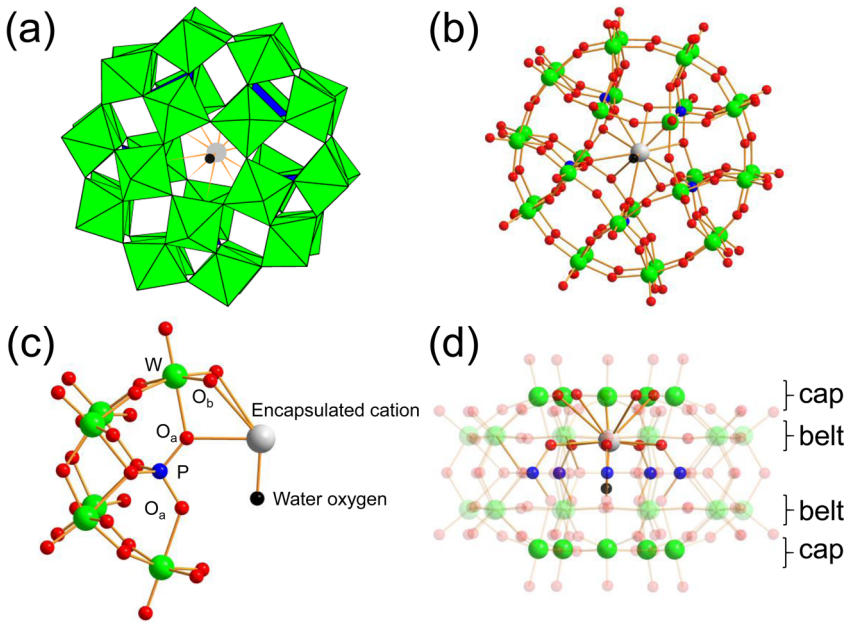

Figure 1. (a) Polyhedral and (b) ball-and-stick representation of a monocation-encapsulated Preyssler-type phosphotungstate molecule. (c) Ball-and-stick representation of one-fifth of the Preyssler-type phosphotungstate ($[PW_6O_{22}]$ unit) with a cation and a coordinating water molecule. (d) Side view of (b). Green, blue, red, gray, and black balls indicate W, P, O, encapsulated cation, and water coordinating to the cation, respectively.

Table 1. Crystal Data of 1a and 1c

Compound	$K_{13}[P_5W_{30}O_{110}K_2]\cdot 26H_2O$ (**1a**)	$H_{13}[P_5W_{30}O_{110}K_2]\cdot 20DMSO\cdot 1H_2O$ (**1c**)
Empirical formula	$K_{13}P_5W_{30}O_{136}H_{52}$	$K_2P_5W_{30}O_{130}C_{40}H_{120}S_{20}$
Molecular weight/g·mol^{-1}	8148.37	9071.08
Crystal size/mm	0.100 × 0.060 × 0.040	0.200 × 0.090 × 0.080
Crystal color and shape	Colorless, prism	Colorless, prism
Temperature/K	100	100
Crystal system	Orthorhombic	Monoclinic
Space group (no.)	*Pnna* (52)	*C*2/*c* (15)
a/Å	32.843(6)	22.601(9)
b/Å	21.455(4)	30.731(13)
c/Å	19.126(4)	28.208(14)
β/deg		94.4770(7)
Volume/Å^3	13477(5)	19532(14)
Z	4	4
Data/parameters	15430/461	22342/1006
R(int)	0.1531	0.0621
Density (calcd)/g·cm^{-1}	4.016	3.084
Abs coefficient/mm^{-1}	26.023	17.992
R_1 ($I > 2\sigma(I)$)[a]	0.1038	0.0400
wR_2 (all data)[b]	0.2224	0.0952

[a] $R_1 = \sum||F_0| - |F_c||/\sum|F_0|$. [b] $R_w = [\sum w(F_0^2 - F_c^2)^2]/\sum[w(F_0^2)^2]^{1/2}$.

stability, redox potential, and acid catalyst property were compared with those of other monocation containing compounds. Furthermore, the arrangement of Preyssler molecules was observed by high-resolution high-angle annular dark-field scanning transmission electron microscopy (HAADF-STEM).

EXPERIMENTAL SECTION

Materials. All chemicals were reagent-grade and used as supplied. Homemade deionized water (Millipore, Elix) was used. The compound $K_{12}[P_5W_{30}O_{110}Bi(H_2O)]\cdot 24H_2O$ was prepared according to the published procedure[13] and analyzed by ^{31}P NMR and IR spectroscopy. All other chemicals were reagent-grade and used as supplied.

*Preparation of $K_{13}[P_5W_{30}O_{110}K_2]\cdot 26H_2O$ (**1a**).* $K_{12}[P_5W_{30}O_{110}Bi(H_2O)]\cdot 24H_2O$ (2.46 g, W: 9 mmol) and KCl (1.34 g, 18 mmol) were mixed in potassium acetate buffer (2 M KOAc and 2 M AcOH being mixed, 5 mL, pH 4.7) in a 30 mL Teflon-lined autoclave, and the mixture was stirred for 5 min at room temperature. The autoclave was placed in an oven heated at 170 °C for 24 h. After the reactor had been cooled down to room temperature, the resulting needle-like colorless crystals were separated from the solution by filtration. The crystals were recrystallized from 5 mL of hot water heated at 90 °C (by a metal bath) to form crystals suitable for single crystal X-ray diffraction analysis. The colorless crystals were collected by filtration and dried at 70 °C overnight (1.00 g, 0.13 mmol, yield of 44% based on W). Elemental anal. calcd (found) for $K_{13}[P_5W_{30}O_{110}K_2]\cdot 26H_2O$: P, 1.83 (1.86); W, 65.0 (64.7); K, 6.91 (7.02); H, 0.62 (0.55) %.

DOI: 10.1021/acs.inorgchem.6b02116
Inorg. Chem. XXXX, XXX, XXX−XXX

*Preparation of $H_{13}[P_5W_{30}O_{110}K_2]\cdot 39H_2O$ (**1b**).* $K_{13}[P_5W_{30}O_{110}K_2]\cdot 26H_2O$ (1.20 g) was dissolved in H_2O (15 mL) and passed through 10 g of Dowex 50 WX8 in the proton form packed in a glass tube (inner diameter: 20 mm) with additional water until the outcoming eluent became neutral, and the obtained eluent was evaporated by using a rotary evaporator *in vacuo* at 333 K. A minimum amount water was added, and the resulting solution was poured into a glass beaker and dried at 70 °C overnight (1.04 g, 0.13 mmol, yield of 93% based on W). Elemental anal. calcd (found) for $H_{13}[P_5W_{30}O_{110}K_2]\cdot 39H_2O$: P, 1.88 (1.93); W, 67.1 (66.9); K, 0.95 (0.81); H, 1.12 (1.11) %.

*Preparation of Crystals of $H_{13}[P_5W_{30}O_{110}K_2]\cdot 20DMSO\cdot 1H_2O$ (**1c**).* $H_{13}[P_5W_{30}O_{110}K_2]\cdot 39H_2O$ (0.40 g) was dissolved in DMSO (0.1 mL) under heating at 70 °C by using an oil bath. After the reactor had been cooled down to room temperature, single crystals suitable for single-crystal X-ray diffraction analysis were obtained. Formula: Elemental anal. Calcd (found) for $H_{13}[P_5W_{30}O_{110}K_2]\cdot 20DMSO\cdot 1H_2O$: H, 1.49 (1.43); C, 5.28 (5.33); S, 7.05 (7.02) %.

X-ray Crystallography. Single-crystal X-ray diffraction data of crystals **1a** and **1c** were collected with a Rigaku Saturn724 diffractometer at 100 K using multilayer mirror monochromated Mo Kα radiation (λ = 0.71075 Å). Data were collected and processed using CrystalClear data collection and processing software (Rigaku Co. Tokyo). An empirical absorption correction was applied and resulted in transmission factors ranging from 0.260 to 0.353 for **1a** and 0147 to 0.237 for **1c**. The data were corrected for Lorentz and polarization effects. The structure was solved by direct methods[26] and expanded using Fourier techniques. All cationic atoms (P, W, K) in the Preyssler-type molecules and some other atoms were refined anisotropically. The other atoms were refined isotropically. The hydrogen atoms of crystal water and DMSO molecules were not located. All calculations were performed using the CrystalStructure 4.2 crystallographic software package (Rigaku Co. Tokyo) except for refinement, which was performed using SHELXL version 2013/4.[27] The numbers of potassium atoms and water oxygen atoms determined by XRD were smaller than those determined by elemental analysis. The data set was corrected with the program SQUEEZE,[28] a part of the PLATON package of crystallographic software used to calculate the solvent or counterion disorder area and to remove its contribution to the overall intensity data, and some water molecules and potassium atoms were omitted by the Platon SQUEEZE procedure. Crystallographic data are summarized in Table 1. Further details of the crystal structure investigation can be obtained from Fachinformationszentrum Karlsruhe, 76344 Eggenstein-Leopoldshafen, Germany (fax: +49-7247-808-666; e-mail: crysdata@fiz-karlsruhe.de; http://www.fiz-karlsruhe.de/request_for_deposited_data.html on quoting the deposition number CSD-431654 and 431653 for $K_{13}[P_5W_{30}O_{110}K_2]$ (**1a**) and $H_{13}[P_5W_{30}O_{110}K_2]$ (**1c**), respectively.

Other Analytical Techniques. Infrared (IR) spectra were recorded on a NICOLET 6700 FT-IR spectrometer (Thermo Fisher Scientific) as KBr pellets. Cyclic voltammetry was performed on a CHI620D system (BAS Inc.) at ambient temperature. A glassy carbon working electrode (diameter, 3 mm), a platinum wire counter electrode, and an Ag/AgCl reference electrode (203 mV vs NHE at 25 °C) (3 M NaCl, BAS Inc.) were used. Approximate formal potential values ($E_{1/2}$ values) were calculated from the CVs as the average of cathodic and anodic peak potentials for corresponding oxidation and reduction waves. ^{31}P NMR spectra were recorded on a Varian system 500 (500 MHz) spectrometer (Agilent) (P resonance frequency: 202.333 MHz). The spectra were referenced to external 85% H_3PO_4 (0 ppm). ^{183}W NMR spectra were recorded on a Varian system 500 (500 MHz) spectrometer (Agilent) (P resonance frequency: 202.333 MHz) (W resonance frequency: 20.825 MHz). The spectrum was referenced to external saturated Na_2WO_4 (0 ppm). The sample of **1a** for ^{183}W NMR spectroscopy was treated with lithium resin in order to increase solubility in D_2O. Elemental analyses were carried out by Mikroanalytisches Labor Pascher (Remagen, Germany). High-resolution ESI-MS spectra were recorded on an LTQ Orbitrap XL (Thermo Fisher Scientific) with an accuracy of 3 ppm. Each sample (5 mg) was dissolved in 5 mL of H_2O, and the solutions were diluted by CH_3CN (final concentration: ca. 10 μg/mL). HAADF-STEM images were obtained with an ARM-200F electron microscope (JEOL, Japan) operated at 200 kV with a CEOS probe aberration corrector. The probe convergence semiangle was 14 mrad, and the collection angle of the HAADF detector was 54−175 mrad. Obtained images were treated with a Local 2D Wiener Filter in the HREM-Filters Pro software (HREM Research Inc., Japan) for noise removal.

Hydrolysis of Ethyl Acetate. Hydrolysis of ethyl acetate was carried out at 353 K with 5 wt % ethyl acetate in D_2O (total volume: 3.0 mL, ethyl acetate: 0.15 g) for 2 h.[25] The amount of protons used was kept at 0.042 mmol.

Conversion and yield were estimated using ^{1}H NMR. From ^{1}H NMR, peaks corresponding to ethyl acetate, ethyl alcohol, and acetic acid were observed. No other peak was observed. Therefore, we assumed that the selectivity of this hydrolysis was 100%. Since peaks of methylene (CH_2O) for ethyl acetate (4.03) and ethyl alcohol (3.52) were well separated, the conversion of ethyl acetate was calculated using the integration ratio of these two peaks as follows:

$$\text{Conversion} = (\text{integration of } CH_2O \text{ of ethyl alcohol}) / (\text{integration of } CH_2O \text{ of ethyl acetate} + \text{integration of } CH_2O \text{ of ethyl alcohol})$$

^{1}H NMR of ethyl acetate in D_2O (HOD peak at 4.75 ppm): 1.13 ppm ($C\underline{H}_3CH_2$, triplet, 3H), 1.97 ppm (CH_3CO, singlet, 3H), 4.03 ppm (CH_2O, quartet, 2H)

^{1}H NMR of ethyl alcohol in D_2O (HOD peak at 4.75 ppm): 1.06 ppm ($C\underline{H}_3CH_2$, triplet, 3H), 3.52 ppm (CH_2O, quartet, 2H).

^{1}H NMR of acetic acid in D_2O (HOD peak at 4.75 ppm): 1.97 ppm (CH_3CO, singlet, 3H).

Electronic Structure Calculations. Density functional theory (DFT) calculations were carried out on the $[K_2P_5W_{30}O_{110}]$ and $[Na(H_2O)P_5W_{30}O_{110}]$ structures with the ADF 2014 suite of programs.[29,30] Equilibrium geometries were obtained upon full geometry optimizations with tight convergence criteria[31] and the OPBE functional[32,33] with an atomic triple-ζ + double polarization basis set, using the frozen core approximation for the following shells: 1s-3p for K, 1s-2p for Na and P, and 1s-4f for W and 1s for O. We simulated an aqueous solution (dielectric constant, ε = 78.39) by including the solvent + counterion effects by means of the *conductor-like screening model*[34−37] (COSMO).

RESULTS AND DISCUSSION

Preparation and Isolation of $[P_5W_{30}O_{110}K_2]^{13-}$. $K_{12}[P_5W_{30}O_{110}Bi(H_2O)]$ was dissolved in acetate buffer (pH 4.7) with an excess amount of K^+ and heated at 170 °C for 24 h. After the reaction mixture had been cooled down to room temperature, a colorless solid was obtained. ^{31}P NMR spectra of the solid show a singlet at −10.96 ppm (Figure 2(b)), and ^{31}P NMR of the filtrate show two singlets at 0.75 and −11.47 ppm (Figure 2(a)), and no peak corresponding to the starting $[P_5W_{30}O_{110}Bi(H_2O)]^{12-}$ (−8.11 ppm) was observed. The singlet at 0.75 ppm may correspond to phosphate related species, and characterization of species showing the singlet at −11.47 ppm is described below. Recrystallization of the solid from hot water produced colorless crystals of potassium salt (**1a**) in ca. 44% yield, showing the same ^{31}P NMR signal as that of the isolated solid (Figure 2(c)).

The crystals (**1a**) were dissolved in water and treated with H^+-resin to produce an acid form (**1b**) showing the same ^{31}P NMR signal as that of **1a** (Figure 2(d)). Recrystallization of **1b** from hot dimethyl sulfoxide (DMSO) produced colorless single crystals (**1c**).

*Characterization of $[P_5W_{30}O_{110}K_2]^{13-}$: Single Crystal Structure Analysis of **1a** and **1c**.* Single-crystal structure analysis of **1a** and **1c** revealed that both colorless crystals

DOI: 10.1021/acs.inorgchem.6b02116
Inorg. Chem. XXXX, XXX, XXX−XXX

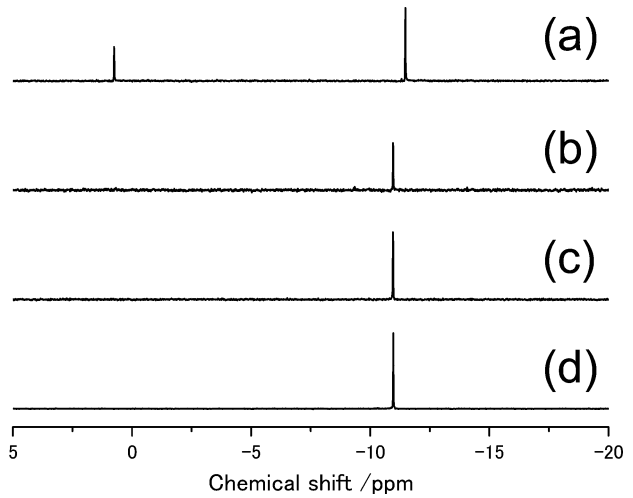

Figure 2. ^{31}P NMR of (a) solution and (b) solid (ca. 50 mg dissolved in 1 mL of D_2O) obtained after the reaction of $K_{12}[P_5W_{30}O_{110}Bi(H_2O)]$ in KOAc buffer (pH 4.7) in the presence of KCl, (c) recrystallized $K_{13}[P_5W_{30}O_{110}K_2]$, and (d) $H_{13}[P_5W_{30}O_{110}K_2]$ dissolved in D_2O (50 mg with 1 mL).

contain a Preyssler-type phosphotungstate and two encapsulated potassium cations (Figure 3(a), (b), and (c)). K^+ in both complexes is placed on the pseudo 5-fold rotation axis of the molecules and coordinated by five oxygens of P−O_a with bond distances of 2.692−2.727 Å and five oxygens of bridging W−O_b−W with bond distances of 2.834−2.941 Å. No water molecule coordinating to K^+ was found. **1a** and **1c** crystallized in orthorhombic and monoclinic space groups, respectively, and counter cations and solvent molecules are located between the molecules (Figure 3(d) and (e)).

It has been reported that the distance between the encapsulated metal cation and the equatorial plane is increased by increasing the positive charge of the encapsulated cation in the case of monocation-encapsulated compounds.[14] However, distances between K^+ and the equatorial plane in mono-K^+-encapsulated compounds[7,8] are not the same as those in mono-$Na^+(H_2O)$ or $Ag^+(H_2O)$-encapsulated compounds (Figure S1 and Table S1), probably due to larger ionic radii of K^+ than those of Na^+. In the case of **1a** and **1c**, the distances between K^+ and the equatorial plane are 1.638 and 1.647 Å, respectively, being similar to those in mono-K^+-encapsulated compounds (Figure S1 and Table S1).

The powder XRD patterns of **1a** and **1c** showed many undefined peaks, indicating that the crystallinity decreased by evaporation of crystal solvents to produce complex mixtures of several crystal phases and amorphous compounds (Figure S2).

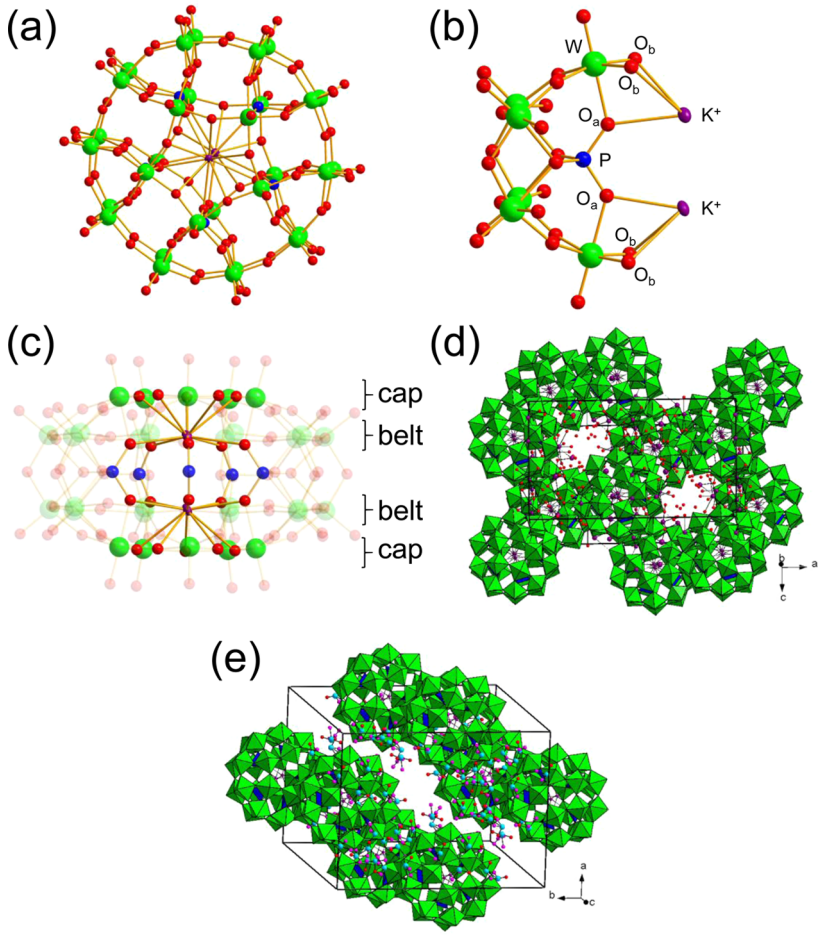

Figure 3. (a) Ball-and-stick representation of a di-K^+-encapsulated Preyssler-type phosphotungstate molecule, (b) one-fifth of the Preyssler-type phosphotungstate ($[PW_6O_{22}]$ unit) with two encapsulated K^+ ions, and (c) side view of (a). (d) Polyhedral presentation of packing of (d) $K_{13}[P_5W_{30}O_{110}K_2]\cdot nH_2O$ (**1a**) and (e) $H_{13}[P_5W_{30}O_{110}K_2]\cdot nH_2O\cdot m$DMSO (**1c**) in a unit cell. Green, blue, red, violet, sky blue, and pink balls indicate W, P, O, encapsulated K^+, S, and C, respectively.

DOI: 10.1021/acs.inorgchem.6b02116
Inorg. Chem. XXXX, XXX, XXX−XXX

Characterization of $[P_5W_{30}O_{110}K_2]^{13-}$: Elemental Analysis, HR-ESI-MS Spectroscopy, ^{183}W NMR, and IR. Elemental analysis revealed that the formulas for **1a** and **1b** are $K_{13}[P_5W_{30}O_{110}K_2]\cdot 26H_2O$ and $H_{13}[P_5W_{30}O_{110}K_2]\cdot 39H_2O$, respectively. HR-ESI-MS of both **1a** and **1b** showed peaks characteristic for $H_7[P_5W_{30}O_{110}K_2]^{6-}$ and $H_8[P_5W_{30}O_{110}K_2]^{5-}$ (Figure S3), indicating the presence of $[P_5W_{30}O_{110}K_2]^{13-}$ species also in solution.

^{183}W NMR of both **1a** and **1b** showed two singlets with a 2:1 integration ratio (Figure 4(a) and (b)). Mono-Na(H_2O)-encapsulated Preyssler-type phosphotungstate shows four singlets with a 2:2:1:1 integration ratio (Figure 4(c) and (d)), because the monocation-encapsulated Preyssler-type phosphotungstate has C_{5v} symmetry, and belt and cap tungstens close to the encapsulated Na^+ are not equivalent to those far from the encapsulated Na^+ (Figure 1(d)), respectively. However, the presence of two singlets with a 2:1 integration ratio indicates that both cap and belt tungstens are equivalent (Figure 3(c)), and the molecule has D_{5h} symmetry with two encapsulated K^+.

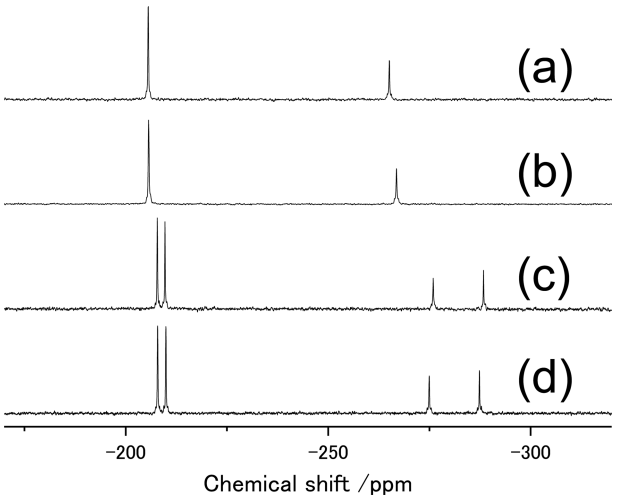

Figure 4. ^{183}W NMR of (a) $K_{13}[P_5W_{30}O_{110}K_2]$ (**1a**), (b) $H_{13}[P_5W_{30}O_{110}K_2]$ (**1b**), (c) $K_{14}[P_5W_{30}O_{110}Na]$, and (d) $H_{14}[P_5W_{30}O_{110}Na]$. Each sample (ca. 1.0 g) was dissolved in ca. 2.5 mL of D_2O. The potassium salts were dissolved using Li-resin.

These results indicate that the isolated Preyssler-type phosphotungstate with two encapsulated K^+ ions is stable in an aqueous solution.

IR spectra of **1a**, **1b**, and **1c** show characteristic spectra for Preyssler-type phoshotungstate with bands at 1178, 1087, 1016, 987, 936, 909, and 785 cm^{-1} (Figure 5), and the spectra are similar to those of mono-$Na^+(H_2O)$-encapsulated Preysser-type phosphotungstates with bands at 1165, 1081, 1018, 983, 935, 912, and 784 cm^{-1}. Two bands corresponding to the P−O stretching region are shifted to a higher wavenumber compared to those of mono-$Na^+(H_2O)$-encapsulated compounds. The IR absorption bands of di-K^+-encapsulated compounds are sharper than those of mono-$Na^+(H_2O)$-encapsulated compounds, because the higher symmetry of the di-K^+ compound gives fewer peaks with many degenerate normal modes of vibration than the $Na^+(H_2O)$-encapsulated compound.

In parallel, constrained geometry optimizations for the di-K^+ and mono-$Na^+(H_2O)$ structures were carried out with the D_5 and C_1 symmetry point groups, respectively (Cartesian coordinates in Table S2). Such reduced symmetries with respect to the idealized D_{5h} and C_s ones have been previously reported to arise from structural distortions of the pseudo-Jahn−Teller[38] type observed in the equatorial loops of the $W_{30}O_{90}$ external framework,[4,14] also known as the *alternating bond length* feature, most accentuated in polyoxomolybdates.[39] As a matter of fact, the D_5 form of the di-K^+ system shows a HOMO−LUMO gap that is 0.22 eV wider than the D_{5h} counterpart, evidence of this phenomenon.

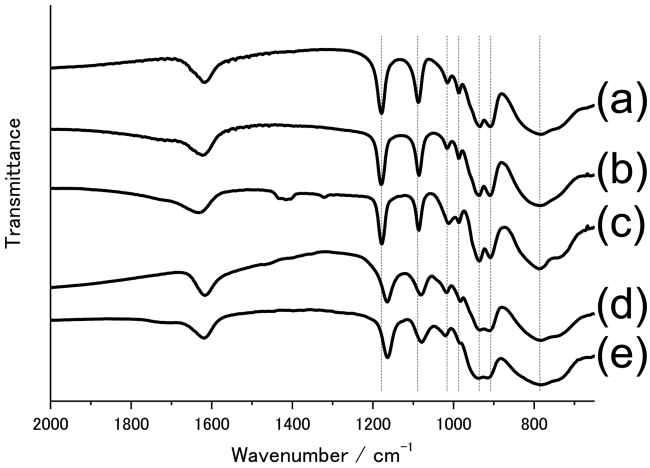

Figure 5. IR of (a) $K_{13}[P_5W_{30}O_{110}K_2]$ (**1a**), (b) $H_{13}[P_5W_{30}O_{110}K_2]$ (**1b**), (c) $H_{13}[P_5W_{30}O_{110}K_2]\cdot$DMSO (**1c**), (d) $K_{14}[P_5W_{30}O_{110}Na]$, and (e) $H_{14}[P_5W_{30}O_{110}Na]$.

Vibrational analysis was then carried out on the D_5 and C_1 optimized structures using the analytical second derivatives program[40−42] implemented in ADF. The IR spectra of Anderson-like,[43] Wells-Dawson,[44] and Keggin structures,[45] $M'M_6O_{24}$, $P_2M_{18}O_{62}$, and $XM_{12}O_{40}$, respectively, have recently been theoretically characterized. Also, the IR spectrum of $SiW_{12}O_{40}$ deposited on Au(111) was obtained from periodic DFT calculations.[46] In our present calculations, no imaginary frequencies were obtained for the structures indicated above, proving that they are true energy minima. For comparison, analogous optimization + frequency calculations performed on the undistorted D_{5h} form of $[P_5W_{30}O_{110}K_2]$ showed that this form is not an energy minimum because it lies 18.4 kcal mol^{-1} higher in energy than the D_5 form and also since it presents six imaginary frequencies with numerical values ranging from −170 to −45 cm^{-1}. The computed frequencies and intensities are summarized in Table S3. The resulting computed vibrational spectra below 1700 cm^{-1} are very similar for di-K^+ and mono-$Na^+(H_2O)$ structures, as can be seen in Figure S4 and Table 2. We found the expected PO_4 stretchings in the 1150−1065 cm^{-1} region in both systems, W═O_{term} stretchings in the 910−830 cm^{-1} region, W−O_{bridge} stretchings in the 830−600 cm^{-1} region, W−O_{bridge} bendings in the 510−300 cm^{-1} region, and W═O_{term} bendings below 300 cm^{-1}. For the di-K^+ structure, calculations gave a coupled PO_4 + W═O_{term} bending at 283 cm^{-1}. In the mono-$Na^+(H_2O)$ compound, two frequencies associated with H_2O vibrations were found at 636 and 184 cm^{-1}. Finally, the encapsulated cation displacements resonate at around 80−100 cm^{-1} for the di-K^+ structure and 85 cm^{-1} for the mono-$Na(H_2O)$ structure.

Analysis of a Side Product. A side product showing a ^{31}P NMR singlet at −11.47 ppm was isolated by cooling the filtrate in a refrigerator (Figure S5(a)). An IR spectrum (Figure S5(b)) indicates the presence of a monolacunary Keggin-type phosphotungstate, $[PW_{11}O_{39}]^{7-}$, and HR-ESI-MS shows

DOI: 10.1021/acs.inorgchem.6b02116
Inorg. Chem. XXXX, XXX, XXX−XXX

Table 2. Computed IR-Active Molecular Vibrations: Frequencies and Intensities for $[P_5W_{30}O_{110}K_2]$ and $[P_5W_{30}O_{110}Na(H_2O)]$

$[P_5W_{30}O_{110}K_2]$			$[P_5W_{30}O_{110}Na(H_2O)]$		
Freq[a]	Intens.[b]	Assignment[c]	Freq[a]	Intens.[b]	Assignment[c]
			1580	<200	H_2O bd
1150	5144	PO_4 st	1147	5264	PO_4 st
			1134	305	PO_4 st
			1115	97	$W{=}O_{term}$, W_2O st
1073	1304	PO_4 st	1066	1251	PO_4 st/bd
			1064	934	PO_4 st/bd
			1059	402	PO_4 st/bd
999	379	$W{=}O_{term}$, PO_4 st	998	361	$W{=}O_{term}$, PO_4 st
			998	371	$W{=}O_{term}$, PO_4 st
911	9266	$W{=}O_{term}$ st	901	4330	$W{=}O_{term}$ st
892	3718	$W{=}O_{term}$, PO_4 st	890–892	3500	$W{=}O_{term}$, PO_4 st
830	1420	$W{=}O_{term}$, $W{-}O_{bridge}$ st	829	1075	$W{=}O_{term}$, $W{-}O_{bridge}$ st
740	927	$W{-}O_{bridge}$ st	744	1179	$W{-}O_{bridge}$ st
717	26585	$W{-}O_{bridge}$ st	724	26676	$W{-}O_{bridge}$ st
672	6015	$W{-}O_{bridge}$ st	678	3068	$W{-}O_{bridge}$ st
652	1299	$W{-}O_{bridge}$ st	659	1298	$W{-}O_{bridge}$ st
648	12900	$W{-}O_{bridge}$ st	649	10151	$W{-}O_{bridge}$ st
			636	5190	H_2O rc
629	2747	$W{-}O_{bridge}$ st	631	1730	$W{-}O_{bridge}$ st
594	11330	$W{-}O_{bridge}$ st	605	10809	$W{-}O_{bridge}$ st
510	1214	$W{-}O_{bridge}$ bd	507	1414	$W{-}O_{bridge}$ bd
344–300	1500–3200	$W{-}O_{bridge}$ bd	345–309	1420–2480	$W{-}O_{bridge}$ bd
283	1730	PO_4, $W{=}O_{term}$ bd	297	1821	H_2O rc
226	1254	$W{=}O_{term}$ bd	223	1198	$W{=}O_{term}$ bd
			184	670	H_2O rc
80–100	<200	K displacements	85	<200	Na displacement

[a]Values in cm^{-1}. [b]Values in km mol^{-1}. [c]St: stretching, Bd: bending, Rc: rocking.

peaks corresponding to a compound with a monolacunary Keggin-type phosphotungstate and a Bi^{3+}, $[(PW_{11}O_{39})\text{-}Bi]^{4-}$ (Figure S3(g)). Although further structural investigation of this side product, including single crystal structure analysis, is still needed, the mono-$Bi^{3+}(H_2O)$-encapsulated starting compound, $K_{12}[P_5W_{30}O_{110}Bi(H_2O)]$, is decomposed to a monolacunary Keggin-type phosphotungstate derivative under the reaction conditions.

Reaction Conditions. For the purpose of producing this di-K^+ species, the $Bi^{3+}(H_2O)$-encapsulated compound $K_{12}[P_5W_{30}O_{110}Bi(H_2O)]$ was better than an $Na^+(H_2O)$-encapsulated compound, $K_{14}[P_5W_{30}O_{110}Na(H_2O)]$. The same reaction with the $Na^+(H_2O)$-encapsulated compound, $K_{14}[P_5W_{30}O_{110}Na(H_2O)]$, did not produce the new solid sample, and the Na-encapsulated compound was recovered (Figure S6).

Sun's group reported mono-$K^+(H_2O)$-encapsulated compounds obtained by a reaction of a mono-$Na^+(H_2O)$-encapsulated compound under a hydrothermal condition.[7,8] However, we were not able to obtain the mono-$K^+(H_2O)$-encapsulated species. One reason might be the difference in concentrations of K^+ in the reaction mixtures. The concentration of K^+ in our reaction system was much higher than that in Sun's reaction conditions. Further investigation to understand the reaction mechanism is now underway by our group.

Redox Potentials. It is known that redox potentials are shifted by changing encapsulated cation charges,[5] and it would be interesting to compare the redox potential of our di-K^+-encapsulated compound with those of monocation-encapsulated compounds.

It has been reported that the $Na^+(H_2O)$-encapsulated Preyssler-type phosphotungstate shows two larger redox couples and one smaller redox couple in 1.0 M HCl corresponding to 4-, 4-, and 2-electron redox of the tungstens, respectively (Figure 6(red)).[5,23] The larger two 4-electron redox couples are split into two 2-electron redox couples by exchanging Na^+ with higher valence cations such as Ca^{2+}, Y^{3+}, or Th^{4+}, and the first 2-electron reduction potential (the most

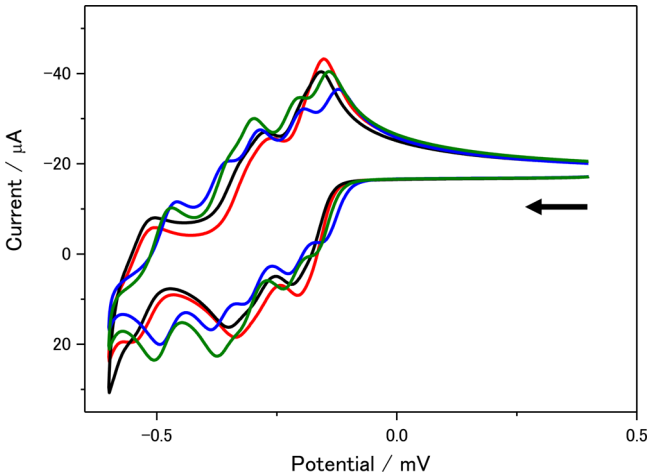

Figure 6. Cyclic voltammograms of (red) $K_{13}[P_5W_{30}O_{110}K_2]$ (**1a**), (black) $K_{14}[P_5W_{30}O_{110}Na]$, (green) $K_{13}[P_5W_{30}O_{110}Ca]$, and (blue) $K_{12}[P_5W_{30}O_{110}Bi]$. Each sample (ca. 1 mM) was dissolved in 1.0 M HCl. The arrow indicates direction of the potential scan and the scan rate was 25 $mV{\cdot}s^{-1}$.

DOI: 10.1021/acs.inorgchem.6b02116
Inorg. Chem. XXXX, XXX, XXX−XXX

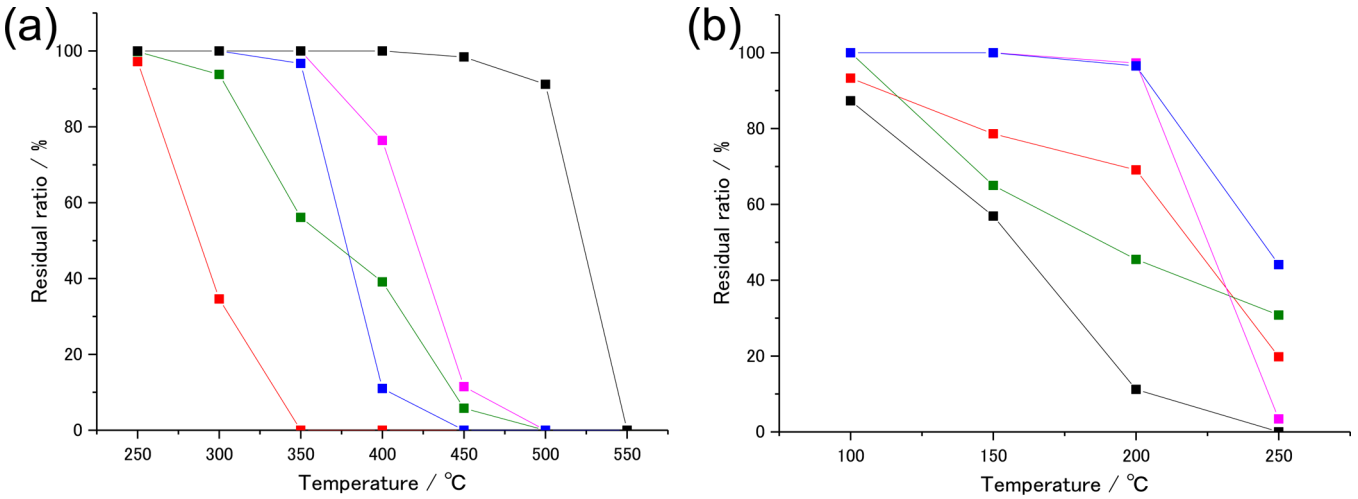

Figure 7. Thermal stabilities of (a) potassium salts and (b) the acidic form of (black) $[P_5W_{30}O_{110}K_2]^{13-}$, (red) $[P_5W_{30}O_{110}Na]^{14-}$, (green) $[P_5W_{30}O_{110}Ca]^{13-}$, (pink) $[P_5W_{30}O_{110}Eu]^{12-}$, and (blue) $[P_5W_{30}O_{110}Bi]^{12-}$. After heating the samples, ^{31}P NMR of the samples dissolved in D_2O was measured. The residual ratio was calculated by the following equation: residual ratio = (integration of the ^{31}P NMR peak assignable to the Preyssler-type phosphotungstate)/(sum of integrations of all ^{31}P NMR peaks). The thermal stability was also confirmed by IR spectra (Figure S8).

positive redox couple) is shifted to a more positive potential by increasing the cationic valence of the encapsulated cations (the first redox potentials are −0.16, −0.14, and −0.12 V vs Ag/AgCl for $Na^+(H_2O)$-, $Ca^{2+}(H_2O)$-, and $Bi^{3+}(H_2O)$-encapsulated compounds, respectively). A cyclic voltammogram of **1a** in 1.0 M HCl shows two larger redox couples and one smaller redox couple that is similar to that of the $Na^+(H_2O)$-encapsulated compound, and the redox potentials are also similar (the first redox potential is −0.15 V vs Ag/AgCl) (Figure 6 (black)). The first redox potential is similar to that of an $Na^+(H_2O)$-encapsulated one.

The redox potential of the di-K^+-encapsulated compound is not the same as that of the mono-$Ca^{2+}(H_2O)$-encapsulated compound but is the same as that of the mono-$Na^+(H_2O)$-encapsulated compound in 1.0 M HCl. Pope's group reported that protonation of the inner oxygen of monocation-encapsulated Preyssler-type phosphotungstates occurs to form a monocation-and-proton-encapsulated species (eq 1),[14] and they reported that the pK_a value is less than 3 for a mono-$Eu^{3+}(H_2O)$-encapsulated compound. We have reported that the pK_a value is ca. 6 for a mono-$Ca^{2+}(H_2O)$-encapsulated compound,[13] and López and Poblet's group reported that the pK_a value is less than 2 for a mono-$Na^+(H_2O)$-encapsulated compound.[18] Inner oxygens (Oa) not coordinating to the encapsulated cations were suggested to be protonated.[14,18]

$$[P_5W_{30}O_{110}M^{n+}]^{(15-n)-} + H^+ = [P_5W_{30}O_{110}M^{n+}H]^{(14-n)-} \quad (1)$$

The inner oxygen of a monocation-encapsulated compound is protonated in 1.0 M HCl, and we consider the observed redox potentials to be those for a protonated species. It is known that the redox potential depends on the negative charge of heteropolytungstate.[47] In the case of **1a**, all inner oxygens (Oa) are already coordinating to K^+ and there is no inner-protonation, and the negative charge of **1a** is 13-, the same as the negative charge of a monoproton-$Na^+(H_2O)$-encapsulated compound. Therefore, the redox potential of **1a** is similar to that of a mono-$Na^+(H_2O)$-encapsulated compound in 1.0 M HCl. Further investigation of redox potentials is now underway by our group.

Thermal Stability. We have reported that the potassium salt of a mono-$Na^+(H_2O)$-encapsulated compound starts to decompose with heating at 300 °C[13] and that the thermal stability is enhanced by exchanging encapsulated cations (Figure 7). The thermal stability of **1a** is maintained up to 450 °C, a higher temperature than that for other Preyssler compounds, and the thermal stability of the potassium salt of the Preyssler-type phosphotungstate is enhanced by encapsulation of two potassium cations in the molecule.

On the other hand, the acid form **1b** is less stable than the acid compounds of other Preyssler compounds and starts to decompose at ca. 100 °C. Therefore, heating of **1b** at a higher temperature is avoided for the isolation process.

TG-DTA analysis of **1a** and **1b** showed gradual weight losses with endothermal peaks up to ca. 400 °C which correspond to water evaporations (Figure S7).

Catalytic Activity as an Acid Catalyst. The acid form **1b** shows catalytic activity similar to that of other acid forms of monocation-encapsulated compounds[13] for hydration of ethyl acetate (Table 3), and the catalytic activity per weight is better than that of the well-known Keggin-type phosphotungstic acid, $H_3PW_{12}O_{40}$. The acid strength estimated by ^{31}P NMR of **1b** is

Table 3. Catalytic Activities for Hydrolysis of Ethyl Acetate[a]

Catalyst	Conv. [%]	Rate: Per weight [mmol g^{-1} min^{-1}]	Rate: Per acid amount [mmol (acid·mol)$^{-1}$ min^{-1}]
$H_{14}[P_5W_{30}O_{110}Na]$[b]	46.2	275.7	164.0
$H_{13}[P_5W_{30}O_{110}Ca]$[b]	48.2	257.0	171.3
$H_{12}[P_5W_{30}O_{110}Eu]$[b]	50.2	258.5	178.5
$H_{12}[P_5W_{30}O_{110}Bi]$[b]	51.2	254.9	182.1
$H_{13}[P_5W_{30}O_{110}K_2]$	55.1	304.8	195.9
$H_3PW_{12}O_{40}$[b]	49.1	175.2	174.5
Blank[b]	1.4		

[a]Amount of protons: 0.042 mmol, 5 wt % ethyl acetate in D_2O (total volume: 3.0 mL, ethyl acetate: 0.15 g), reaction temperature: 353 K, reaction time: 2 h. [b]Data from our previous paper.[13]

DOI: 10.1021/acs.inorgchem.6b02116
Inorg. Chem. XXXX, XXX, XXX−XXX

similar to that of the acid forms of other Preyssler-type compounds (Figure S9).

HAADF-STEM Image. Recently, observation of polyoxotungstate molecules using high-resolution high-angle annular dark-field scanning transmission electron microscopy (HAADF-STEM) has attracted much attention.[48,49] Figure 8 shows the arrangements of Preyssler molecules in **1a**. Doughnut-shaped Preyssler molecules with a diameter of 1.2 nm and thickness of 0.7 nm (Figure 8(c)) are observed. It is obvious that the observed *a* and *c* axes are shorter than those obtained by single crystal structure analysis, indicating that the *a* and *c* axes are reduced by evaporation of water between the Preyssler molecules under a highly vacuumed condition in STEM observation. This is the first TEM observation of Preyssler-type molecules. It is known that samples should be stable against an electron beam and heat generated on samples by irradiation of an electron beam. Enhanced thermal stability might help observation of Preyssler-type molecules.

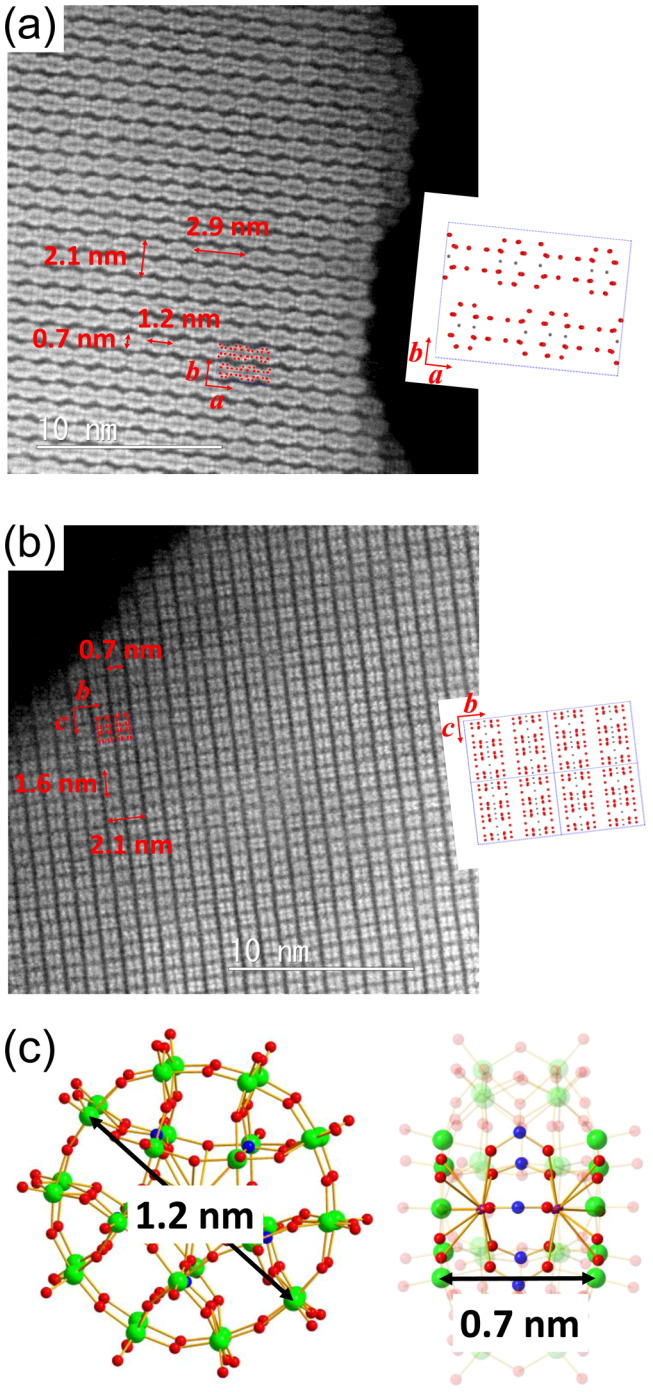

Figure 8. High-resolution HAADF-STEM images of **1a** along the (a) *c* axis and (b) *a* axis and arrangement of tungsten atoms (red balls) in the corresponding plane estimated by reduction of *a* and *c* lattice lengths to 2.9 and 1.6 nm, respectively, from the crystal structure of **1a**. The sample was heated at 100 °C before observation. (c) Model and distances of Preyssler molecules. The heaviest atom, W, is observed as a white spot in the HAADF-STEM images. Therefore, distances between tungsten atoms are indicated.

CONCLUSION

The first Preyssler-type phosphotungstate with two encapsulated cations, $[P_5W_{30}O_{110}K_2]^{13-}$, was prepared as a potassium salt and an acid form and was characterized by single crystal structure analysis, elemental analysis, ^{31}P NMR, ^{183}W NMR, IR, CV, DFT calculations, and ESI-MS. The potassium salt shows higher thermal stability than that of other Preyssler-type phosphotungstates, and the acid form shows catalytic activity similar to other phosphotungstates for hydration of ethyl acetate. Furthermore, the arrangement of Preyssler molecules can be observed by HAADF-STEM.

ASSOCIATED CONTENT

Supporting Information

The Supporting Information is available free of charge on the ACS Publications website at DOI: 10.1021/acs.inorgchem.6b02116.

Distance between encapsulated cations and equatorial plane. Powder XRD of **1a** and **1c**. ESI-MS results. IR and computed IR of **1a** and $K_{14}[P_5W_{30}O_{110}Na(H_2O)]$. ^{31}P NMR and IR of a side product. ^{31}P NMR of the solution obtained after reaction of $K_{14}[P_5W_{30}O_{110}Na(H_2O)]$ in KOAc buffer (pH 4.7) in the presence of KCl. TG-DTA of **1a** and **1b**. IR of **1a** and **1b** after heating. Acid strength of **1b** estimated using ^{31}P NMR chemical shift. Selected bond lengths in Preyssler-type phosphotungstates. List of Cartesian coordinates for the DFT optimized $[K_2P_5W_{30}O_{110}]$ and $[Na(H_2O)P_5W_{30}O_{110}]$ structures. List of computed IR frequencies and intensities (PDF)
CIF data for **1a** (CIF)
CIF data for **1c** (CIF)

AUTHOR INFORMATION

Corresponding Author

*Masahiro Sadakane, E-mail: sadakane09@hiroshima-u.ac.jp; Fax: +81 82 424 5494; Tel: +81 82 424 4456.

Notes

The authors declare no competing financial interest.

ACKNOWLEDGMENTS

MS is grateful for Grants-in-Aid for Scientific Research (Scientific Research "C", grant no. 26420787) from the Ministry of Education, Culture, Sports, and Science, Japan, and A-STEP program of the Japanese Science and Technology Agency (JST), and Furukawa Foundation for Promotion of Technology. XL is grateful to the Spanish Ministry of Science and Innovation (MICINN) (project CTQ2014-52774-P), the DGR of the Generalitat de Catalunya (grant no. 2014SGR199), and the XRQTC. The electron microscopy study by NH was

DOI: 10.1021/acs.inorgchem.6b02116
Inorg. Chem. XXXX, XXX, XXX−XXX

supported by JSPS KAKENHI Grant Number JP16K06863. We thank T. Amimoto and N. Kawata at the Natural Science Center for Basic Research and Development (N-BARD), Hiroshima University, for the ESI-MS measurement and initial single crystal X-ray structure analysis, respectively.

REFERENCES

(1) Pope, M. T. *Heteropoly and Isopoly Oxometalates*; Springer-Verlag: Berlin, 1983.
(2) Hill, C. L. Thematic issue on Polyoxometalates. *Chem. Rev.* **1998**, *98*, 1−390.
(3) Cronin, L. Thematic Issue on Polyoxometalates. *Chem. Soc. Rev.* **2012**, *41*, 7325−7648.
(4) Alizadeh, M. H.; Harmalker, S. P.; Jeannin, Y.; Martin-Frère, J.; Pope, M. T. A Heteropolyanion with Fivefold Molecular Symmetry That Contains a Nonlabile Encapsulated Sodium Ion. The Structure and Chemistry of $[NaP_5W_{30}O_{110}]^{14-}$. *J. Am. Chem. Soc.* **1985**, *107*, 2662−2669.
(5) Creaser, I.; Heckel, M. C.; Neitz, R. J.; Pope, M. T. Rigid Nonlabile Polyoxometalate Cryptates $[ZP_5W_{30}O_{110}]^{(15-n)-}$ That Exhibit Unprecedented Selectivity for Certain Lanthanide and Other Multivalent Cations. *Inorg. Chem.* **1993**, *32*, 1573−1578.
(6) Liang, M.-X.; Ruan, C.-Z.; Sun, D.; Kong, X.-J.; Ren, Y.-P.; Long, L.-S.; Huang, R.-B.; Zhen, L.-S. Solvothermal Synthesis of Four Polyoxometalate-Based Coordination Polymer Including Diverse Ag(I)-π Interactions. *Inorg. Chem.* **2014**, *53*, 897−902.
(7) Hu, T.-P.; Zhao, Y.-Q.; Jaglicic, Z.; Yu, K.; Wang, X.-P.; Sun, D. Four Hybrid Materials Based on Preyssler P5W30 Polyoxometalate and Frist-Row Transition-Metal Complex. *Inorg. Chem.* **2015**, *54*, 7415−7423.
(8) Zhao, Y.-Q.; Yu, K.; Wang, L.-W.; Wang, Y.; Wang, X.-P.; Sun, D. Anion-Induced Supramolecular Isomerization in Two Preyssler P5W30 Polyoxometalate-Based Hybrid Materials. *Inorg. Chem.* **2014**, *53*, 11046−11050.
(9) Dickman, M. H.; Gama, G. J.; Kim, K.-C.; Pope, M. T. The Structure of Europium(III)- and Uranium(IV) Derivatives of $[P_5W_{30}O_{110}]^{15-}$: Evidence for "Cryptohydration". *J. Cluster Sci.* **1996**, *7*, 567−583.
(10) Williams, C. W.; Antonio, M. R.; Soderholm, L. The formation and stability of $[EuP_5W_{30}O_{110}]^{12-}$ and $[AmP_5W_{30}O_{110}]^{12-}$. *J. Alloys Compd.* **2000**, *303*−*304*, 509−513.
(11) Antonio, M. R.; Soderholm, L. Cerium Valence in Cerium-Exchanged Preyssler's Heteropolyanion through X-ray Absorption Near-Edge Structure. *Inorg. Chem.* **1994**, *33*, 5988−5993.
(12) Granadeiro, C. M.; de Castro, B.; Balula, S. S.; Cunha-Silva, L. Lanthanopolyoxometalates: From the structure of polyanions to the design of functional materials. *Polyhedron* **2013**, *52*, 10−24.
(13) Takahashi, K.; Sano, T.; Sadakane, M. Preparation and characterization of Preyssler-type phosphotungstic acid, $H_{15-n}[P_5W_{30}O_{110}M^{n+}]$, with different encapsulated cations (M = Na, Ca, Bi, Eu, Y, or Ce), and their thermal stability and acid catalyst properties. *Z. Anorg. Allg. Chem.* **2014**, *640*, 1314−1321.
(14) Kim, K.-C.; Pope, M. T.; Gama, G. J.; Dickman, M. H. Slow Proton Exchange in Aqueous Solution. Consequences of Protonation and Hydration within the Central Cavity of Preyssler Anion Derivatives, $[lM(H_2O)lP_5W_{30}O_{110}]^{n-}$. *J. Am. Chem. Soc.* **1999**, *121*, 11164−11170.
(15) Hayashi, A.; Haioka, T.; Takahashi, K.; Bassil, B. S.; Kortz, U.; Sano, T.; Sadakane, M. Cation effect on formation of Preyssler-type 30-tungsto-5-phosphate: enhanced yield of Na-encapsulated derivative and direct synthesis of Ca- and Bi-encapsulated derivatives. *Z. Anorg. Allg. Chem.* **2015**, *641*, 2670−2676.
(16) Antonio, M. R.; Chiang, M.-H. Stabilization of Plutonium(III) in the Preyssler Polyoxometalate. *Inorg. Chem.* **2008**, *47*, 8278−8285.
(17) Cardona-Serra, S.; Clemente-Juan, J. M.; Coronado, E.; Gaita-Arino, A.; Camon, A.; Evangelisti, M.; Luis, F.; Martines-Perez, M. J.; Sere, J. Lanthanoid Single-Ion Magnets Based on Polyoxometalates with a 5-fold Symmetry: The Series $[LnP_5W_{30}O_{110}]^{12-}$ (Ln^{3+} = Tb, Dy, Ho, Er, Tm, and Yb). *J. Am. Chem. Soc.* **2012**, *134*, 14982−14990.
(18) Fernández, J. A.; López, X.; Bo, C.; de Graaf, C.; Baerends, E. J.; Poblet, J. M. Polyoxometaltes with Internal Cavities: Redox Activity, Basicity and Cation Encapsulation in $[X^{n+}P_5W_{30}O_{110}]^{(15-n)-}$ Preyssler Complexes, with X = Na^+, Ca^{2+}, Y^{3+}, La^{3+}, Ce^{3+}, and Th^{4+}. *J. Am. Chem. Soc.* **2007**, *129*, 12244−12253.
(19) Antonio, M. R.; Soderholm, L. Implications of the unusual redox behavior exhibited by the heteropolyanion $[EuP_5W_{30}O_{110}]^{12-}$. *J. Alloys Compd.* **1997**, *250*, 541−543.
(20) Soderholm, L.; Liu, G. K.; Muntean, J.; Malinsky, J.; Antonio, M. R. Coordination and Valence of Europium in the Heteropolyanion $[EuP_5W_{30}O_{110}]^{12-}$. *J. Phys. Chem.* **1995**, *99*, 9611−9616.
(21) Antonio, M. R.; Soderholm, L. Redox Behavior of Europium in the Preyssler Heteropolyanion $[EuP_5W_{30}O_{110}]^{12-}$. *J. Cluster Sci.* **1996**, *7*, 585−591.
(22) Antonio, M. R.; Soderholm, L.; Williams, C. W.; Ullah, N.; Francesconi, L. C. Redox behavior of cerium in heteropolyoxotungstate complexes. *J. Chem. Soc., Dalton Trans.* **1999**, 3825−3830.
(23) Chiang, M.-H.; Antonio, M. R.; Soderholm, L. Energetics of the Preyssler anion's molecular orbitals: quantifying the effect of the encapsulated-cation's charge. *Dalton Trans.* **2004**, 3562−3567.
(24) Zhang, Z.-M.; Yao, S.; Li, Y.-G.; Han, X.-B.; Su, Z.-M.; Wang, Z.-S.; Wang, E.-B. Inorganic Crown Ethers: Sulfate-Based Preyssler Polyoxometalates. *Chem. - Eur. J.* **2012**, *18*, 9184−9188.
(25) Sadakane, M.; Ichi, Y.; Ide, Y.; Sano, T. Thermal Stability and Acidic Strength of Preyssler-Type Phosphotungstic Acid, $H_{14}[P_5W_{30}O_{110}Na]$ and It's Catalytic Activity for Hydrolysis of Alkyl Acetates. *Z. Anorg. Allg. Chem.* **2011**, *637*, 2120−2124.
(26) Burla, M. C.; Caliandro, R.; Camalli, M.; Carrozzini, B.; Cascarano, G. L.; Giacovazzo, C.; Mallamo, M.; Mazzone, A.; Polidori, G.; Spagna, R. SIR2011: a new package for crystal structure determination and refinement. *J. Appl. Crystallogr.* **2012**, *45*, 357−361.
(27) Sheldrick, G. M. A short history of SHELX. *Acta Crystallogr., Sect. A: Found. Crystallogr.* **2008**, *A64*, 112−122.
(28) van der Sluis, P.; Spek, A. L. BYPASS: an effective method for the refinement of crystal structures containing disordered solvent regions. *Acta Crystallogr., Sect. A: Found. Crystallogr.* **1990**, *46*, 194−201.
(29) Fonseca Guerra, C.; Snijders, J. G.; Te Velde, G.; Baerends, E. J. Towards an order-N DFT method. *Theor. Chem. Acc.* **1998**, *99*, 391−403.
(30) Te Velde, G.; Bickelhaupt, F. M.; van Gisbergen, S. J. A.; Fonseca Guerra, C.; Baerends, E. J.; Snijders, J. G.; Ziegler, T. Chemistry with ADF. *J. Comput. Chem.* **2001**, *22*, 931−967.
(31) Optimized structures must be very accurate when frequency calculations are to be conducted, since molecular vibrations can be highly dependent on geometrical parameters.
(32) Handy, N. C.; Cohen, A. J. Left-right correlation energy. *Mol. Phys.* **2001**, *99*, 403−412.
(33) Swart, M.; Ehler, A. W.; Lammertsma, K. Performance of the OPBE exchange-correlation functional. *Mol. Phys.* **2004**, *102*, 2467−2474.
(34) Klamt, A.; Schüürmann, G. COSMO: a new approach to dielectric screening in solvents with explicit expressions for the screening energy and its gradient. *J. Chem. Soc., Perkin Trans. 2* **1993**, *2*, 799−805.
(35) Andzelm, J.; Kölmel, C.; Klamt, A. Incorporation of solvent effects into density functional calculations of molecular energies and geometries. *J. Chem. Phys.* **1995**, *103*, 9312−20.
(36) Klamt, A. Conductor-like Screening Model for Real Solvents: A New Approach to the Quantitative Calculation of Solvation Phenomena. *J. Phys. Chem.* **1995**, *99*, 2224−35.
(37) Pye, C. C.; Ziegler, T. An implementation of the condutor-like screening model of solvation within the Amsterdam density functional package. *Theor. Chem. Acc.* **1999**, *101*, 396−408.
(38) Bersuker, I. *The Jahn Teller Effect*; Cambridge University Press: Cambridge, 2006.

DOI: 10.1021/acs.inorgchem.6b02116
Inorg. Chem. XXXX, XXX, XXX−XXX

(39) Yan, L.; López, X.; Carbó, J. J.; Sniatynsky, R. T.; Duncan, D. D.; Phoblet, J. M. On the Origin of Alternating Bond Distortions and the Emergence of Chirality in Polyoxometalate Anions. *J. Am. Chem. Soc.* **2008**, *130*, 8223−8233.
(40) Berces, A.; Dickson, R. M.; Fan, L.; Jacobson, H.; Swerhone, D.; Ziegler, T. An implementaion of the coupled perturbed Kohn-Sham equations: perturbation due to nuclear displacements. *Comput. Phys. Commun.* **1997**, *100*, 247−262.
(41) Jacobsen, H.; Berces, A.; Swerhone, D.; Ziegler, T. Analytic second derivatives of molecular energies: a density functional implementation. *Comput. Phys. Commun.* **1997**, *100*, 263−276.
(42) Wolff, S. K. Analytical second derivatives in the Amsterdam density functional package. *Int. J. Quantum Chem.* **2005**, *104*, 645−659.
(43) Davantès, A.; Costa, D.; Lefèvre, G. Infrared Study of (Poly)tungstate Ions in Solution and Sorbed into Layered Double Hydroxides: Vibrational Calculations and In Situ Analysis. *J. Phys. Chem. C* **2015**, *119*, 12356−12364.
(44) Zhang, F.-Q.; Guan, W.; Tan, L.-K.; Zhang, T.-T.; Xu, M.-T.; Hayfron-Benjamin, E.; Su, Z.-M. On the Origin of the Relative Stability of Wells−Dawson Isomers: A DFT Study of α-, β-, γ-, α*-, β*-, and γ*-$[(PO_4)_2W_{18}O_{54}]^{6-}$ Anions. *Inorg. Chem.* **2011**, *50*, 4967−4977.
(45) Clavería-Cádiz, F.; Arratia-Pérez, R.; MacLeod-Carey, D. Density functional study on Keggin heteropolyanions containing fifth period main group heteroatoms. *Polyhedron* **2016**, *117*, 478−186.
(46) Aparicio-Anglès, X.; Clotet, A.; Bo, C.; Poblet, J. M. Towards the computational modelling of polyoxoanions on metal surfaces: IR spectrum characterisation of $[SiW_{12}O_{40}]^{4+}$ on Ag(111). *Phys. Chem. Chem. Phys.* **2011**, *13*, 15143−15147.
(47) Sadakane, M.; Steckhan, E. Electrochemical Properties of Polyoxometalates as Electrocatalysts. *Chem. Rev.* **1998**, *98*, 219−237.
(48) Hiyoshi, N.; Kamiya, Y. Observation of microporous cesium salts of 12-tungsosilicic acid using scanning transmission electron microscopy. *Chem. Commun.* **2015**, *51*, 9975−9978.
(49) Zhang, Z.; Sadakane, M.; Hiyoshi, N.; Yoshida, A.; Hara, M.; Ueda, W. Acidic Ultrafine Tungsten Oxide Molecular Wires for Cellulosic Biomas Conversion. *Angew. Chem., Int. Ed.* **2016**, *55*, 10234−10238.

DOI: 10.1021/acs.inorgchem.6b02116
Inorg. Chem. XXXX, XXX, XXX−XXX